Earth Surf. Dynam., 3, 483–499, 2015
www.earth-surf-dynam.net/3/483/2015/
doi:10.5194/esurf-3-483-2015

Earth Surface Dynamics
Open Access

Topographic roughness as a signature of the emergence of bedrock in eroding landscapes

D. T. Milodowski, S. M. Mudd, and E. T. A. Mitchard

School of GeoSciences, University of Edinburgh, Edinburgh, UK

Correspondence to: D. T. Milodowski (d.t.milodowski@ed.ac.uk)

Received: 12 March 2015 – Published in Earth Surf. Dynam. Discuss.: 18 May 2015
Revised: 10 September 2015 – Accepted: 1 October 2015 – Published: 16 October 2015

Abstract. Rock is exposed at the Earth surface when rates of erosion locally exceed rates of soil production. The thinning of soils and emergence of bedrock has implications spanning geomorphology, ecology and hydrology. Soil-mantled hillslopes are typically shaped by diffusion-like sediment transport processes that act to smooth topography through time, generating the familiar smooth, convex hillslope profiles that are common in low relief landscapes. Other processes, however, can roughen the landscape. Bedrock emergence can produce rough terrain; in this contribution we exploit the contrast between rough patches of bedrock outcrop and smooth, diffusion-dominated soil to detect bedrock outcrops. Specifically, we demonstrate that the local variability of surface normal vectors, measured from 1 m resolution airborne LiDAR data, can be used as a topographic signature to identify areas within landscapes where rock exposure is present. We then use this roughness metric to investigate the transition from soil-mantled to bedrock hillslopes as erosion rates increase in two transient landscapes, Bald Rock Basin, which drains into the Middle Fork Feather River, California, and Harrington Creek, a tributary of the Salmon River, Idaho. Rather than being abrupt, as predicted by traditional soil production models, in both cases the transition from fully soil-mantled to bedrock hillslopes is gradual and spatially heterogeneous, with rapidly eroding hillslopes supporting a patchwork of bedrock and soil that is well documented by changes in topographic roughness, highlighting the utility of this metric for testing hypotheses concerning the emergence of bedrock and adding to a growing body of evidence that indicates the persistence of partial soil mantles in steep, rapidly eroding landscapes.

1 Introduction

The geomorphic transition from hillslopes with a continuous soil mantle to rugged bedrock is a key phase in the evolution of eroding landscapes. Many slowly eroding landscapes feature sediment transport processes that act to diffuse and dampen short wavelength features of the topography, generating smooth, soil-mantled hillslopes (Gilbert, 1909; Carson and Kirkby, 1972). Bedrock becomes exposed at the surface when the rate of erosion exceeds the maximum rate of soil production (Carson and Kirkby, 1972; Heimsath et al., 1997, 2012). This transition is gradual, and spatially variable, reflecting the fact that both soil production and sediment transport are spatially heterogeneous, and typically operate via discrete events (Wilkinson et al., 2005; Strudley et al., 2006a, b; Gabet and Mudd, 2010; Furbish and Roering, 2013). The emergence of bedrock signifies a fundamental change in the dynamics of sediment transport, which become increasingly stochastic as mobile colluvium is stripped away and the hillslope sediment flux becomes detachment limited (e.g. Binnie et al., 2007). Furthermore, the establishment of terrestrial ecosystems is dependent on a hospitable substrate: the mosaic of bedrock and soil that constitutes the hillslope surface imposes a physical template on the development of terrestrial ecosystems (Phillips and Marion, 2004; Pelletier and Rasmussen, 2009; Gabet and Mudd, 2010; Sheffer et al., 2013). The rate of erosion that is sufficient to completely strip soil may therefore represent a limiting threshold for ecosystem development (Graham et al., 2010). In addition, the presence or absence of bedrock outcrop may reveal important information about the availability of nutrients such as phospho-

rous in soil parent material (Hahm et al., 2014). Equally, the transition between deep and shallower soils, signalled by the appearance of bedrock outcrops, is an ecological gradient allowing for niche specialisation, driving biodiversity and diversity within species, influencing ecosystem function, species creation and adaptability (Smith et al., 1997). Quantifying the spatial distribution of rock exposure and its relationship to the ecological and geomorphological characteristics of a landscape thus comprises an important challenge in understanding critical zone dynamics.

The advent of airborne Light Detection And Ranging (LiDAR) as a remote-sensing technology over the last decade or so has driven a revolution in the fields of both geomorphology and ecology by providing high-resolution (< 1 m) observations of both canopy structure and sub-canopy topography, therefore enabling observations to be made at length-scales sufficiently small to analyse the geomorphic characteristics of hillslopes (Roering et al., 2010; Hurst et al., 2012; DiBiase et al., 2012). Higher resolution still (< 1 cm) is possible using terrestrial LiDAR systems, permitting the analysis of multi-scale dimensionality from length scales of centimetres to several metres, enabling the objective classification of point clouds into specific features, such as vegetation and bedrock, with a high degree of accuracy (Brodu and Lague, 2012; Lague et al., 2013). Despite the obvious benefits of high-resolution terrestrial LiDAR scanning, the greater spatial coverage permitted by airborne surveys maintains its utility for landscape scale applications, requiring the development of remote sensing methods with which it is possible to extract information about the geomorphic characteristics of hillslopes, such as the extent of rock exposure, from such comparatively low-resolution data.

DiBiase et al. (2012) used airborne LiDAR data to investigate the impact of increasing erosion rates on hillslope morphology in the San Gabriel Mountains, CA, demonstrating that slope distributions became increasingly skewed towards higher gradients, as steep, bedrock slopes became increasingly abundant. They successfully developed the Rock Exposure Index (REI) as a topographic metric to map rock exposure in this landscape, defined as areas in which the local gradient exceeds a threshold steepness beyond which soil is no longer retained on the hillslope. DiBiase and Lamb (2013) exploited this metric to quantify sediment storage by vegetation on steep slopes, and thus assess the likely impact of wild fires on hillslope sediment fluxes. Marshall and Roering (2014) used a similar slope-based metric to map erosion-resistant sandstone beds in the Oregon Coast Range.

However, slope-based metrics are not universally applicable. For example, when long-term rates of erosion exceed the local maximum rate of soil production, bedrock will be exposed at the surface, irrespective of slope (Carson and Kirkby, 1972; Heimsath et al., 1997, 2012). Within a given setting, rates of soil production may be limited by factors such as climate, vegetation, lithology and soil thickness (e.g. Pelletier and Rasmussen, 2009; Chorover et al., 2011; Goodfellow et al., 2014a). It is evident that in many landscapes rock exposure emerges in places even at low topographic gradients, and is particularly common in regions with thin regolith cover, where tor formation is common (Anderson, 2002; Strudley et al., 2006b), on ridgelines (Gabet et al., 2015), or where bedrock heterogeneities drive small-scale variation in weathering rates (Goodfellow et al., 2014b).

Another method by which rock exposure might be mapped from high-resolution topographic models of hillslopes is through changes in their textural characteristics. On hillslopes mantled by a veneer of soil, sediment transport is driven by the time-integrated effect of a suite of local-scale diffusive processes, including bioturbation, tree throw, dry ravel and rain splash (e.g. Gabet, 2003; Gabet et al., 2003; Yoo et al., 2005; Furbish et al., 2007). The net efficiency of these processes in transporting material increases with topographic gradient – they are diffusion-like (Furbish et al., 2009) – such that they act to dampen the amplitude of local topography, particularly when viewed at length-scales greater than those at which the dominant sediment transport rates operate. The resultant hillslopes therefore typically exhibit smooth, convex surfaces that are ubiquitous to many soil-mantled landscapes (Gilbert, 1909; Culling, 1963, 1965; Carson and Kirkby, 1972; McKean et al., 1993). The emergence of bedrock at the surface potentially drives a significant increase in roughness, because there is a fundamental change in the dynamics of sediment transport at this location within the landscape: sediment transport is detachment limited (Dietrich et al., 2003) and the local relief structure is governed by the characteristics of the bedrock (fracture density and orientation, bedding and foliation, weathering behaviour).

In this paper we exploit this idea and develop a new technique to identify areas of rock exposure from high-resolution LiDAR data, based on short-wavelength topographic roughness. This method is validated in two granitoid landscapes by comparing the results to rock exposure mapped independently from high-resolution orthophotographs, highlighting its utility and limitations. Finally, as a case study, we apply the algorithm in two strongly transient landscapes – the first in the Feather River region of the northern Sierra Nevada, California; the second in the Salmon River region SW of the Bitterroot Mountains, Idaho – in order to illustrate the transition from diffusive, soil-mantled hillslopes to rough, bedrock hillslopes as erosion rates increase in both settings.

2 Methods – quantifying surface roughness

Sediment fluxes on soil-mantled hillslopes have been shown to be well approximated by a linear relationship with the topographic slope (Carson and Kirkby, 1972), becoming nonlinear as erosion rates increase and steepen hillslopes towards a limiting slope beyond which mobile colluvium is unstable (Roering et al., 1999). The resultant topography is diffusive: hillslope processes act to dampen the amplitude of local

micro-topography generating characteristically smooth hillslope topography. Our method starts from the hypothesis that the emergence of bedrock through the soil mantle should be detectable as an increase in the local roughness of the topographic surface, due to a geomorphic process transition away from diffusion-like hillslope processes.

Specifically we analyse surface roughness using the variability of the orientation of local slope normal vectors, using the eigenvalues of an orientation tensor, derived from the vectors normal to the topographic surface. A similar approach has been used in a range of geological applications, notably in earthquake seismology (Fara and Scheidegger, 1963), analysing trends in geological structural data (Woodcock, 1977) and more recently as a method to objectively locate landslides from high-resolution topographic data (McKean and Roering, 2004). We note here that other metrics describing surface roughness, such as the standard deviation of slope, have been used in other geomorphic contexts, such as LiDAR-based mapping of volcanic deposits (Whelley et al., 2014) and channel bed morphology (Cavalli et al., 2008).

Initially a second order polynomial surface is fitted to a moving data window of 3×3 pixels (Evans, 1980). This method of surface approximation to calculate topographic metrics has been widely utilised in the calculation of surface derivatives, predominately slope and curvature, for the extraction of geomorphic features such as hilltops (Hurst et al., 2012), channel networks (Pirotti and Tarolli, 2010; Sofia et al., 2011), landslides (Tarolli et al., 2010; Lin et al., 2013), and anthropogenic features on floodplains (Sofia et al., 2014). Using a larger length-scale would dampen the roughness signal, but may be necessary if the topographic data are noisy (Sofia et al., 2011). The surface can be described by:

$$z = ax^2 + by^2 + cxy + \mathrm{d}x + ey + f, \tag{1}$$

where z is the surface elevation, x and y are horizontal coordinates, and a, b, c, d, e, and f are empirical fitting coefficients. A similar approach was employed by Hurst et al. (2012) to calculate hilltop curvature, who found no significant difference between the results obtained using six or nine term polynomials in their surface fitting algorithm. Consequently we use a six term polynomial as it maximises computational efficiency. The normal to a surface is given by:

$$\boldsymbol{n} = \nabla(f(x, y) - z). \tag{2}$$

For Eq. (1), using spherical coordinates (r, θ, φ) at the origin, the unit normal vector becomes:

$$\boldsymbol{n} = \left(1, \tan^{-1}\left(\sqrt{d^2 - e^2}\right), \tan^{-1}\left(\frac{e}{d}\right)\right). \tag{3}$$

For N surface normal vectors, the orientation matrix, $\mathbf{T}$, can be constructed using the directional cosines l_i, m_i and n_i, as shown below:

$$\mathbf{T} = \begin{pmatrix} \sum_i^N l_i^2 & \sum_i^N l_i m_i & \sum_i^N l_i n_i \\ \sum_i^N m_i l_i & \sum_i^N m_i^2 & \sum_i^N m_i n_i \\ \sum_i^N n_i l_i & \sum_i^N n_i m_i & \sum_i^N n_i^2 \end{pmatrix}. \tag{4}$$

The orientation matrix can be solved to find the three eigenvectors $\boldsymbol{v}_1$, $\boldsymbol{v}_2$, $\boldsymbol{v}_3$ and their corresponding eigenvalues, λ_1, λ_2, λ_3, which describe the degree of clustering of the normal vectors about the principal axes of the distribution (Watson, 1966). Following Woodcock (1977), we normalise the eigenvalues by the number of observations (N):

$$S_1 = \frac{\lambda_1}{N}, \quad S_2 = \frac{\lambda_2}{N}, \quad S_3 = \frac{\lambda_3}{N}. \tag{5}$$

S_1 ($\frac{1}{3} \leq S_1 \leq 1$) describes the clustering around the major axis, S_2 ($0 \leq S_2 \leq \frac{1}{2}$) the intermediate axis, and S_3 ($0 \leq S_3 \leq \frac{1}{3}$) the minor axis. These normalised eigenvalues can be used to describe the morphology of a given surface (Woodcock, 1977): for a smooth surface, the local surface normal vectors will have similar orientations, thus they will cluster tightly around the major axis, $\boldsymbol{v}_1$, and S_1 will be large, whereas the degree of clustering around the minor axis, $\boldsymbol{v}_3$, will thus be very small (low S_3). Conversely, for a rough surface, the normal vectors will be more randomly orientated; there will be a weaker degree of clustering around $\boldsymbol{v}_1$ (low S_1), whilst the clustering around $\boldsymbol{v}_3$ will be relatively high (therefore high S_3).

A moving data kernel is passed over the data set to analyse the variability of the surface normal vectors within the local (circular) neighbourhood. The radius of this kernel determines the length-scale over which the roughness of the surface is quantified. Identifying the correct length-scale in this case is critical – too large, and long wavelength variations in the topography (i.e. ridge-valley topography) will dominate, obscuring any signal from rock exposure; too small, and then the measured roughness will pick out locally smooth surfaces within an exposure of bedrock. We discuss determining the optimal length-scale in the Validation section (for results, see Sect. 3.4).

3 Validation of the surface roughness algorithm

3.1 Validation sites

In order to test the surface roughness metric described above as a measure of rock exposure, we selected two validation sites in western USA (Fig. 1) based on the availability of co-located LiDAR and high-resolution (< 30 cm) orthophotographs. A further requirement for validation sites was that the degree of vegetation cover was minimal, to permit the objective classification of rock outcrop in the imagery (Sect. 3.2). All LiDAR data sets and orthophotographs used in the study are freely available from either the National Science Foundation's OpenTopography service

Table 1. Summary of data sets used during in this study.

Airborne LiDAR				
Region	Acquisition date	Areal extent used (km^2)	Point Density ($pts\,m^{-2}$)	Data set acknowledgement
Rayleigh Peak, CO	May 2010	23	10.1	1
Poway Creek, CA	Jan 2005	1.4	1.4	2
Bald Rock Basin, CA	Sep 2008	4.0	9.8	1
Harrington Creek, ID	Aug 2011	49.0	4.6	1
Orthophotographs				
Region	Acquisition date	Resolution/m	Sensor type	Data set acknowledgement
Rayleigh Peak, CO	Mar 2010	0.30	Colour Near-Infrared	3
Poway Creek, CA	May 2012	0.15	Colour Near-Infrared	3

1: National Center for Airborne Laser Mapping (NCALM – http://www.ncalm.org); 2: USGS Center for LiDAR Information Coordination and Knowledge (CLICK – http://lidar.cr.usgs.gov/; via OpenTopography); 3: USGS (via EarthExplorer http://earthexplorer.usgs.gov/).

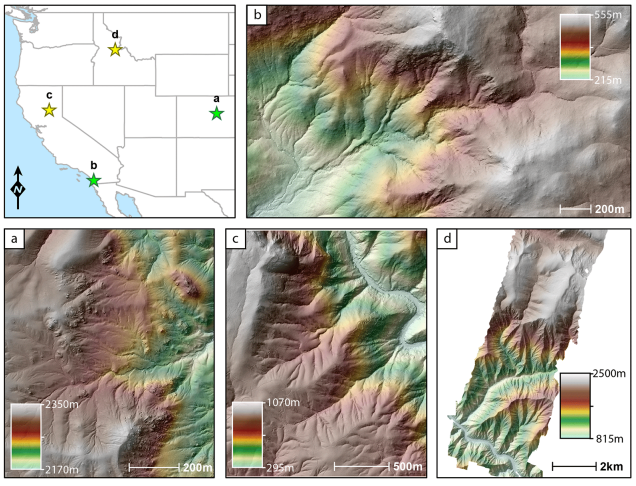

Figure 1. Field sites used in this study; **(a)** headwaters of the Spring Creek catchment, ∼ 2.7 km SW of Rayleigh Peak, in the Colorado Front Ranges; **(b)** Poway Creek, California; **(c)** Bald Rock Basin, draining into the Middle Fork Feather River, Californian Sierra Nevada; **(d)** Harrington Creek, which drains into the Salmon River, Idaho. Sites **(a)** and **(b)** were used to validate our algorithm; sites **(c)** and **(d)** were subsequently analysed to investigate the transition from soil-mantled to bedrock hillslopes in transient landscapes.

(www.opentopography.org) or from the United States Geological Survey (USGS; earthexplorer.usgs.gov/). Technical details for the data sets have been collated in Table 1.

3.1.1 Rayleigh Peak, Colorado

The first validation site is located in the headwaters of the Spring Creek catchment, in the central Colorado Frontal Range, which drains into the South Platte River ∼ 40 km SSW of Denver (Fig. 1a). The climate is semi-arid with frequent intense summer storms. Mean Annual Precipitation (MAP) is 440 mm, and average monthly temperatures varies from a maximum (minimum) of 27.7 (10.8) °C in summer to 6.0 (−9.0) °C in winter (http://www.prismclimate.org). Vegetation comprises grassland and sparse coniferous forest, of which Ponderosa Pine and Douglas Fir are the principal components, the distribution of which is dominated by the impact of the 1996 Buffalo Creek wildfire, in which 79 % of the Spring Creek catchment suffered severe burn damage (Moody and Martin, 2001), so that forest canopy now covers only a small proportion of the landscape. The bedrock geology comprises Pikes Peak Granite (Ruleman et al., 2011), which forms large, blocky outcrops. The degree of rock outcrop at the site varying from almost full exposure on hillslopes around Rayleigh Peak, which dominates the topography, to fully soil-mantled hillslopes that are now predominately covered by grassland.

3.1.2 Poway Creek, California

The second study site is located in the Poway Creek catchment, located just east of the city of Poway, north of San Diego (Fig. 1b). MAP is 825 mm and temperatures typically range from 29.1 (14.1) °C in summer to 11.5 (−0.2) °C in winter (http://www.prismclimate.org). The bedrock geology is principally composed of granodiorite with dacitic-andesitic extrusive rocks underlying the eastern margin (Todd et al., 2004). There is a gradient in rock exposure from predominately soil-mantled, grassy hillslopes that are frequently gullied, to abundant rock outcrop in the steep, rugged headwaters. Due to classification errors in the original data set, the LiDAR point cloud was reclassified using the multi-scale curvature algorithm incorporated within the MCC-LiDAR tool (Evans and Hudak, 2007).

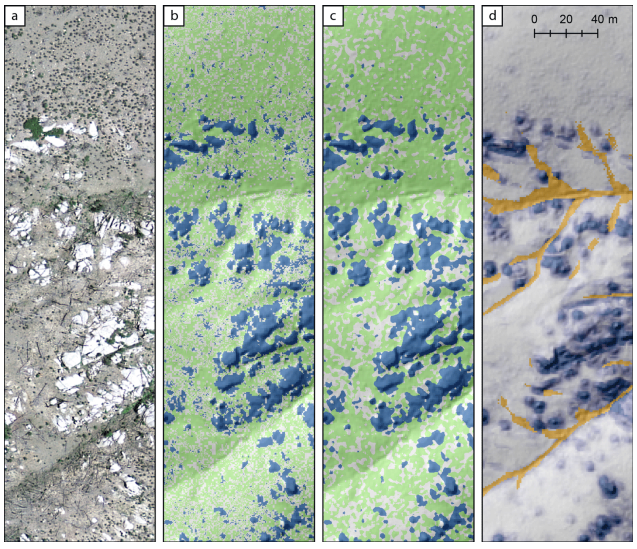

Figure 2. Validation procedure illustrated for the Rayleigh Peak site: **(a)** high-resolution colour near-infrared orthophotograph; **(b)** results from the SVM classification procedure – rock = blue, soil mantled/vegetation = green; **(c)** classified image following the subsequent majority filter; **(d)** map of S_3, which we use as a measure of surface roughness, measured using a neighbourhood window radius of 3 m. Orange pixels mark areas identified as being channelised.

3.2 Objective identification of rock exposure from high-resolution orthophotographs

The high-resolution orthophotographs were classified using the supervised classification toolbox available within the ENVI 4.8 processing environment. Specifically we utilised the Support Vector Machine classification method (Wu et al., 2004), trained using a series of manually selected sample Regions Of Interest (ROIs) for each class. The classes used to analyse each orthophotograph comprised the following: "Rock", "Vegetation", "Bare Earth" and "Shadow". With the exception of the "Shadow" class, which was not as spatially extensive, each ROI had a minimum of 10 000 pixels. The SVM classification was implemented to analyse the imagery at two pyramid levels, with a Pyramid Reclassification Threshold (i.e. the probability threshold required to reclassify a pixel, if given a different class at a finer resolution) of 0.90. As the avoidance of false positives within our validation data set was of paramount importance, pixels were left unclassified if the confidence level for the final class fell below 95 %. Subsequently a 7×7 pixel majority filter was employed to reduce the noise in the classified image Fig. 2. As our focus is on comparing soil-mantled and rocky hillslopes, we combine the vegetation and bare earth classes, and treat areas that are in shadow as unclassified.

The quality of the classification scheme for each image was judged based both with a visual inspection of the classification results to ensure that there were no systematic errors located away from the training ROIs, and using the error matrices for each classification, providing a quantitative assessment of the scheme's ability to correctly reproduce the classification of the initial ROIs. At the 95 % confidence interval, the SVM scheme discarded 9.4 % of the ROI pixels as unclassified in the Rayleigh Peak data set and 12.0 % in the Poway Creek data set. At the Rayleigh Peak site, the classification scheme was able to replicate the rock ROIs with a commission error (ratio of non-rock pixels classified as rock to the total number of pixels in the rock ROI) of 0.23 % and an omission error (ratio of rock pixels incorrectly classified to the total number of pixels in the rock ROI) of 0.01 %. At the Poway Creek site, the ROIs were replicated with a commission error of 0.01 % and an omission error of 0.13 %. Across the region as a whole, both of our validation sites, the classification scheme struggled in areas where there are large changes in the saturation of the imagery (Figs. 3 and 4), due to aspect-driven differences in illumination: as a result some areas have an increased proportion of unclassified pixels. This problem is endemic to image classification in high relief terrain, and is very hard to correct even with good topographic data and bi-directional reflectance function (BDRF-driven) models, as there is often no information captured in the brightest and darkest parts of the image (e.g. Teillet et al., 1982; Colby, 1991; Hale and Rock, 2003). Again, this highlights the potential advantages of landscape classification techniques based on the morphological characteristics of the topographic surface. In addition, it is evident that there are still some areas where the image classification provides an incorrect classification. Nevertheless, the classification is sufficiently successful to provide two large test data sets with which to validate our roughness metric. Errors in the validation data sets will, if anything, lead to an underestimate of the accuracy of our topographically derived metric; it is hard to imagine how errors in the classification could inflate the accuracy of the topographic roughness metric, as the data sets are entirely independent and any errors unlikely to be co-located.

3.3 Validation procedure

We used the rock exposure maps from the classifications described above to perform the validation of the roughness algorithm in each of the four test landscapes. Since channels are often topographically rough, we first restricted our analysis to the hillslope domain. Several methods have been proposed to identify channel pixels in high-resolution topography (e.g. Lashermes et al., 2007; Passalacqua et al., 2010; Pelletier, 2013); in each landscape we have used the method of Lashermes et al. (2007), in which the topography is filtered using a Gaussian filter, and then a curvature threshold to define the extent of the channel network is obtained statistically by looking for the departure from the expectations of a Gaussian distribution. This approach produces visibly satisfactory results across the range of landscapes used here.

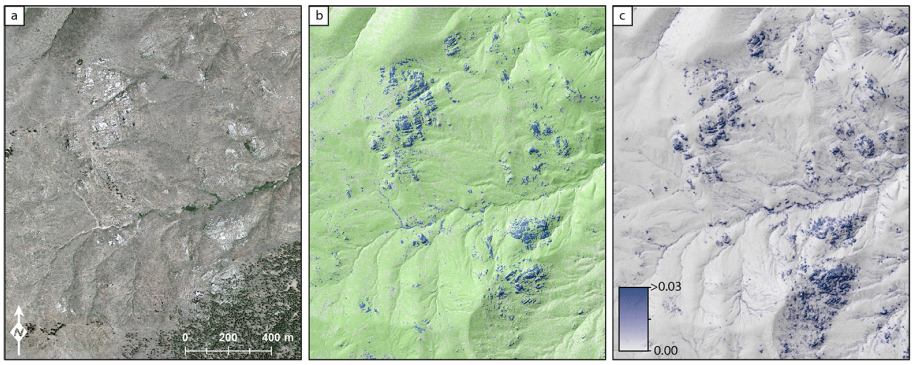

Figure 3. Validation maps for the Rayleigh Peak site: **(a)** high resolution, colour-near infrared orthophotograph; **(b)** results from combined classification procedure: rock = blue, soil mantled/vegetation = green; **(c)** map of S_3, which we use as a measure of surface roughness, measured using a neighbourhood window radius of 3 m. To maximise the clarity of the maps, channelised portions of the landscape have not been masked.

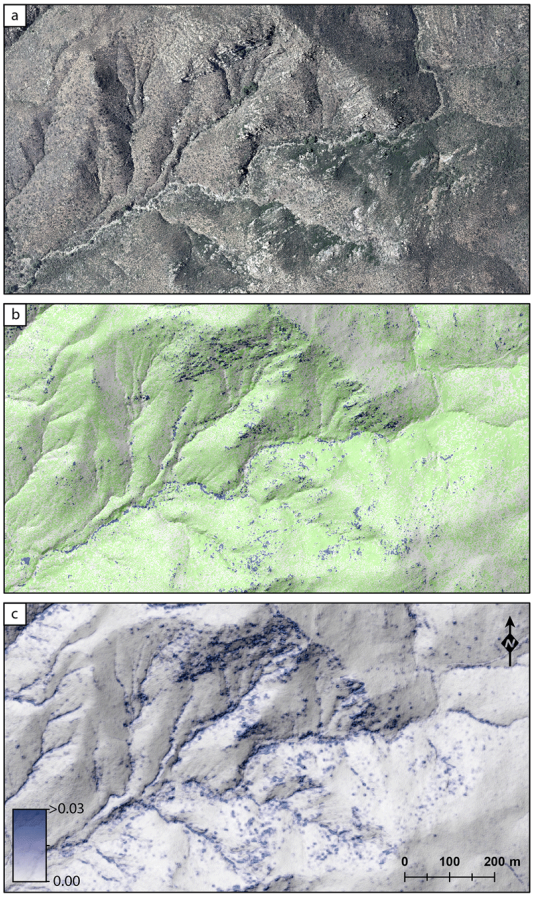

Figure 4. Validation maps for the Poway Creek site: **(a)** high resolution, colour-near infrared orthophotograph; **(b)** results from combined classification procedure: rock = blue, soil mantled/vegetation = green; **(c)** map of S_3, which we use as a measure of surface roughness, measured using a neighbourhood window radius of 3 m. To maximise the clarity of the maps, channelised portions of the landscape have not been masked.

After isolating the hillslopes, we searched through the parameter space for the S_3 eigenvalue, performing a pixel-pixel comparison with the orthophotograph classifications to ascertain whether the algorithm produced a true positive (TP), false positive (FP), true negative (TN) or false negative (FN) for a given roughness threshold. In order to objectively assess the performance of the algorithm and determine an optimum threshold value to delineate areas with rock exposure, we calculated five test statistics: (i) true positive rate (= TP/(TP + FN)); (ii) false positive rate (= FP/(TN+FP)); (iii) commission error (= FP/(TP + FN)); (iv) omission errors (= FN/(TP + FN)); and (v) the overall accuracy (= (TP+TN)/Total); to objectively assess the performance of the algorithm and determine an optimum threshold value to delineate areas with rock exposure. In order to avoid bias in the aforementioned statistics towards either class, the larger of the two classes was randomly subsampled to the same number of test pixels as the smaller of the two before proceeding with the calculations. We repeated this procedure for three neighbourhood radii (3, 5 and 7 m) in each of the two field sites to assess the influence of neighbourhood size on the measured surface roughness. An important consideration when interpreting the validation results is that the surface roughness represents a spatially aggregated metric, representing a blend of the topographic characteristics within the circumference of the neighbourhood window. Consequently, it is unlikely that this metric will discriminate between small areas of patchy soil interspersed between rugged rock outcrops at length scales smaller than the neighbourhood window. This effect becomes increasingly significant as the window size increases and is an inevitable outcome from neighbourhood statistical approaches. As a result, we eliminate from our validation data set areas that are not classed as rock exposure that lie within 7 m (the largest neighbourhood radius used) of mapped rock exposure. For comparison, we also report the same statistics for the full data set.

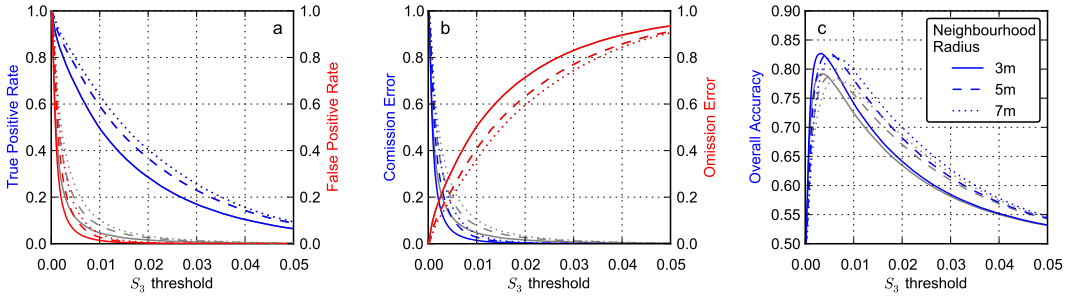

Figure 5. Validation statistics for Rayleigh Peak site as a function of the roughness threshold used to delimit rock exposure for three different neighbourhood window radii: **(a)** true positive and false positive rates; **(b)** commission and omission errors; **(c)** overall accuracy. These tests were conducted twice – the red and blue lines illustrate the results from tests in which the pixels classified as soil-mantled pixels were filtered to avoid localities proximal to rock exposure (see text), therefore is more representative of the roughness signature of a pure soil-mantled hillslope; the grey lines illustrate the same tests, but without this prior filtering step.

3.4 Validation results

In both landscapes, the close correspondence between the topographically derived roughness maps against the rock exposure mapped from the high resolution orthophotographs attests to a qualitatively good agreement between the two (Figs. 3 and 4). Hillslopes that are covered by a continuous mantle of soil map consistently as areas that are topographically smooth, having locally consistent normal vector orientations; in contrast the emergence of bedrock drives a significant increase in the roughness of the affected hillslopes that is clearly picked up by our algorithm.

In the Rayleigh Peak example, both areas with widespread rock outcrop and more isolated exposures are picked out (Fig. 3). The primary area of discordance lies in the SW corner of the image. Here the roughness algorithm predicts a much greater extent of rock exposure than the classified image. Inspection of the orthophotograph in this area reveals significant vegetation cover, obscuring areas where there is clearly bedrock, thus severely hampering the optical classification in this location. Areas of enhanced roughness running laterally along the trunk channel, which flows from west to east here, provide another potential false positive in the roughness map; this highly localised roughness signature marks the banks of the incised channel. The validation statistics similarly show a distinct difference between soil-mantled hillslopes and areas with rock exposure (Fig. 5; Table 2). The FPR rapidly decreases as the value of S_3 used to discriminate between the two characteristics increases, with a maximum accuracy (taking into account both false positives and false negatives) of $>80\,\%$ for $\sim 0.003 \leq S_{3,\,\mathrm{threshold}} \leq \sim 0.005$. The TPR also decreases across this interval, which is likely to be driven by areas of rock exposure where the rock surfaces have a low fracture density, therefore appear smooth, and the fact that our test data set is not perfect (see discussion in Sect. 3.2). We stress here that the imperfections in the validation data set derived from the orthophotographs will lead to a conservative estimate of the true accuracy of the roughness algorithm. Critically from the perspective of mapping out areas of rock exposure, the rate at which the TPR decreases with increasing values of $S_{3,\,\mathrm{threshold}}$ is much lower than that of the FPR. Increasing the size of the neighbourhood window over which the surface roughness is characterised acts to increase the number of true positives for a given threshold, but there is a trade-off, as this improvement is accompanied by an increase in the number of false positives (Figs. 5 and 7; Table 2). This is probably due to the "leakage" of the roughness signal from areas where there is rock exposure into the expanded neighbourhoods of proximal soil pixels (Fig. 7), and also due to the fact that the longer wavelength topographic structure imposed by the ridge-valley architecture starts to influence the variability in the distribution of surface normal vectors; the latter case is particularly prevalent in areas that are located close to gullies and channels.

The pattern that emerges from the Poway Creek site is very similar; again, the maps of rock exposure do a qualitatively good job at locating hillslopes with rock outcrops, although the visual comparison is hindered by the spatially variable success of the classification scheme (Fig. 4). Again, the network of channels and gullies provides additional sources of roughness in the landscape. The performance in the quantitative tests exhibits very similar patterns to those obtained for the Rayleigh Peak site (Fig. 6; Table 2).

3.5 Implications for use of topographic roughness in other settings

The fact that the roughness signatures of both validation landscapes display strikingly similar characteristics (Figs. 5 and 6), suggests that surface roughness is a promising tool for mapping the extent of bedrock outcrop on hillslopes. As with existing methods (e.g. REI; DiBiase et al., 2012), an important caveat is that full calibration is dependent on the a posteriori knowledge of threshold values, obtained, for example, through comparison against rock exposure mapped from high-resolution photographs (DiBiase et

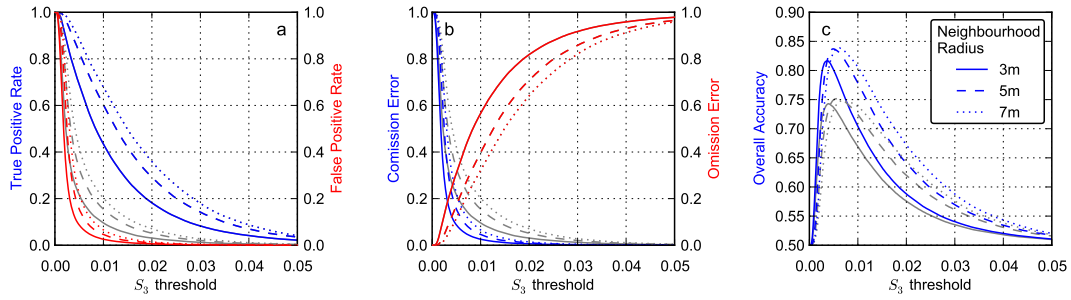

Figure 6. Validation statistics for Poway Creek site as a function of the roughness threshold used to delimit rock exposure for three different neighbourhood window radii: **(a)** true positive and false positive rates; **(b)** commission and omission errors; **(c)** overall accuracy. These tests were conducted twice – the red and blue lines illustrate the results from tests in which the soil-mantled samples were filtered to avoid localities proximal to rock exposure, therefore is more representative of the roughness signature of a pure soil-mantled hillslope; the grey lines illustrate the same tests, but without this prior filtering step.

Table 2. Summary of validation results for three different threshold values of the eigenvalue S_3. These represent a subsample from the data displayed in Figs. 5 and 6. TPR = True Positive Rate; FPR = False Positive Rate; CE = Commission Error; OE = Omission Error; OA = Overall Accuracy (for definitions see text). As the surface roughness metric is spatially aggregated, this pixel-wise comparison was conducted avoiding soil-mantled pixels that were located proximal to areas of rock exposure (see text). Including these results in an increase in the false positive rate and commission errors, and corresponding drop in overall accuracy (see also Figs. 4 and 6); however these errors are collocated with areas of rock exposure, and arise as a consequence of this proximity.

	TPR			FPR			CE			OE			OA		
Neighbourhood Window Radius	3 m	5 m	7 m	3 m	5 m	7 m	3 m	5 m	7 m	3 m	5 m	7 m	3 m	5 m	7 m
$S_{3,\text{threshold}}$	Rayleigh Peak														
0.005	0.68	0.76	0.80	0.05	0.11	0.16	0.05	0.11	0.16	0.32	0.24	0.20	0.81	0.83	0.82
0.010	0.50	0.59	0.64	0.01	0.03	0.04	0.01	0.03	0.04	0.50	0.41	0.36	0.74	0.78	0.80
0.015	0.37	0.46	0.50	< 0.01	0.01	0.01	< 0.01	0.01	0.01	0.63	0.54	0.49	0.68	0.73	0.75
$S_{3,\text{threshold}}$	Poway Creek														
0.005	0.69	0.83	0.88	0.09	0.15	0.23	0.09	0.15	0.23	0.31	0.17	0.12	0.80	0.84	0.83
0.010	0.43	0.60	0.68	0.03	0.05	0.07	0.03	0.05	0.07	0.57	0.40	0.32	0.70	0.78	0.81
0.015	0.28	0.42	0.50	0.01	0.02	0.03	0.01	0.02	0.03	0.72	0.58	0.50	0.63	0.70	0.73

al., 2012; this study). This is non-trivial in areas with significant vegetation cover due to the difficulty in resolving the ground surface; indeed, in areas with significant tree cover a significant portion of exposed rock is always hidden. Greater uncertainty will arise in areas where prior calibration against orthophotographs is not possible. A further element of caution is required, as our validation sites are limited to low-moderate relief, granitoid settings, but nevertheless, we expect that the methodology can be used judiciously in other landscapes. We provide an illustration of the method in a landscape underlain by layered sedimentary rocks in the Supplement. A number of important considerations are necessary in doing so, given that in many scenarios it will not be possible to use aerial imagery to independently judge the performance of the algorithm.

Firstly, it is evident from Figs. 3–6 that a minor portion of landscapes mapped as rock exposure is topographically smooth. Variations in bedrock morphology present a challenge for the textural classification of topography. Errors may be introduced in areas where a significant proportion of the bedrock has been polished, or where the bedrock is massive and exhibits sparse jointing. The latter case is illustrated by smooth, massive granitoid domes, where the distribution of fractures is dominated by surface parallel exfoliation joints (Migon, 2006). In such cases the textural characteristics of bedrock hillslopes may be indistinguishable from those with a continuous soil mantle. In the case of layered rocks, slopes parallel to the structural fabric may be smooth, whereas slopes that cross-cut the layering will appear rougher. This may drive variable accuracy in the results of textural classification metrics. However, large areas of smooth bedrock should be readily visible in satellite/aerial imagery because such conditions are unlikely to support significant vegetation cover (Graham et al., 2010; Hahm et al., 2014). Furthermore, where smooth surfaces form steep structures, a slope-based metric such as the REI (DiBiase et al., 2012) can easily be

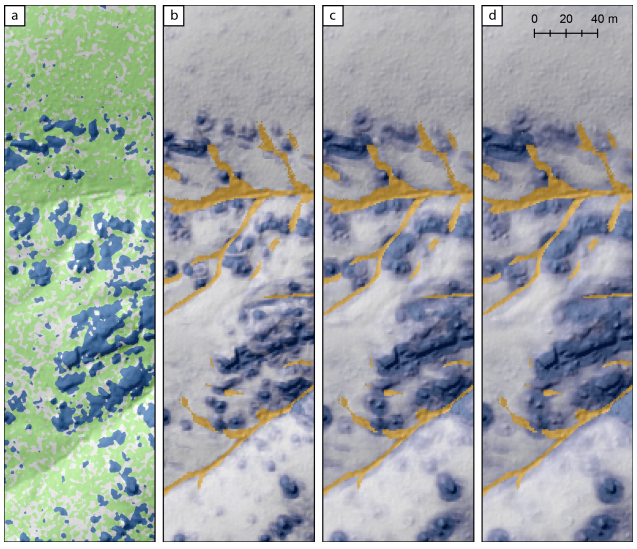

Figure 7. Illustration of the impact of the effect of changing neighbourhood window radius on the roughness signal that is measured: **(a)** results from combined classification procedure – rock = blue, soil mantled/vegetation = green; **(b–d)** maps of S_3 using a neighbourhood window radius of **(a)** 3 m; **(b)** 5 m; and **(c)** 7 m. Orange pixels mark areas identified as being channelised. Note the increase in the leakage of the roughness signal into proximal areas as the neighbourhood radius is increased.

employed alongside surface roughness to catch these false negatives. Combinations of topographic metrics in this way may potentially permit more robust feature extraction from high-resolution data.

Secondly, bedrock exposure is not unique in adding roughness elements to landscapes, as surface roughness may potentially be generated by other processes. At length scales of 11–50 m, topographic roughness may be dominated by the signature of deep seated landslides, if present (Booth et al., 2009), while other features associated with landslides may generate roughness at shorter wavelengths (McKean and Roering, 2004; Tarolli et al., 2010). Roughness at small length scales (typically < 7.5 m) can also be generated via tree throw where this process is prevalent (Roering et al., 2010; Marshall and Roering, 2014). Moreover a degree of familiarity with target landscapes is likely essential in order to critically evaluate the results, although this criteria is not unique to this method. Furthermore, in more complex landscapes with multiple roughness generation mechanisms, the spatial distribution of roughness generated by different processes may still allow useful quantitative information to be extracted (for example, instances of tree throw are likely to be quasi-random, or at least spatially discrete events, whereas exposure of bedrock in hillslopes is likely to generate connected "clusters" of roughness), although we do not extend our analysis in this manner here.

The size of the polynomial surface-fitting window should ideally be comparable to the feature being extracted. In landscapes where other roughening elements are present, or when the LiDAR data are noisy, a larger window can be employed, or the topography can be smoothed, with the limitation that as the degree of smoothing increases, the textural information that distinguished bedrock hillslopes from soil-mantled hillslopes is progressively lost (Albani et al., 2004; Sofia et al., 2013). Finally, the neighbourhood size used to quantify surface roughness will dictate the resolution at which you can discriminate between soil and rock outcrop (Fig. 7).

For many applications, whether making an assessment of shallow landslide hazard, or testing hypotheses concerning the transition from soil-mantled bedrock topography, avoiding false negatives is of paramount importance. For neighbourhood radii of 3–5 m, a threshold value of $S_3 = 0.01$ limits the occurrence of false positives to < 5 % (Fig. 5), decreasing to < 2 % for $S_3 = 0.015$. Omission errors decrease substantially by increasing the radius of the neighbourhood window, but there is a trade-off against an increasing frequency of commission errors (Figs. 5 and 6).

In Fig. 8, we illustrate an alternative approach to mapping rock exposure using the surface roughness metric introduced above. Specifically we assess the fraction of pixels within a local neighbourhood that have a value of S_3 greater than a specified threshold value. Employing a sufficiently high threshold, we can thus express the expected rock exposure within that neighbourhood. This provides a conservative estimate of the degree of rock outcrop for a given portion of hillslope. In all cases, there is a positive correlation between the rock exposure mapped from the orthophotographs and the roughness of the topographic surface (Fig. 8). However, when the S_3 threshold is set too low, the frequency of false positives leads to an overestimation of the rock exposure in a given portion of the landscape, as expected from our previous analysis (Figs. 4–7). In the Rayleigh Peak site, there is a good agreement between the degree of rock exposure mapped by the two methods using an S_3 threshold of 0.010, if roughness is quantified with a neighbourhood radius of 3 m, and 0.015 if quantified with a neighbourhood radius of 5 m. Again this conforms to the expectations arising from the validation tests (Fig. 5). In Poway Creek, there appears to be a systematic over-estimation of the rock exposure. The Poway Creek catchment presents a more challenging landscape to classify for three reasons: (i) gullies are common, and many of the channels show evidence of recent incision; the channel banks in these incised localities generate false positives due to the sharp break in slope. There may be bedrock exposed in the terrace walls, but if present may be obscured by overhanging vegetation. (ii) Changing insolation conditions across the image made classification using the optical data more difficult (Fig. 5). (iii) The original LiDAR point cloud was relatively sparse (Table 1), as a consequence of which discrimination of ground returns from those hitting low lying shrubs is more difficult. As a general point we emphasise

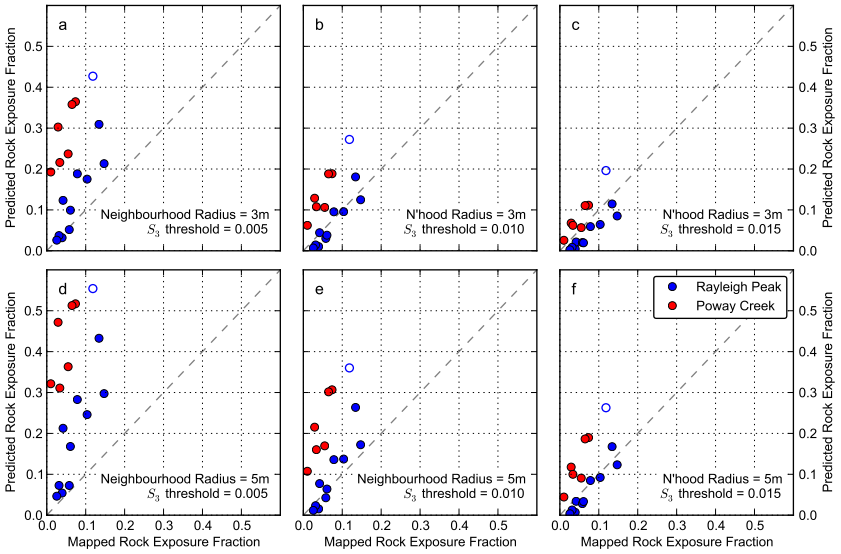

Figure 8. A comparison of the rock exposure classified from the orthophotographs against the expected fraction of rock exposure predicted using different thresholds of the surface roughness metric, S_3, for a series of the validation sites near Rayleigh Peak, Colorado, and Poway Creek, California. Each data point represents the rock exposure mapped within a 401 m × 401 m square region within a regularly spaced grid. **(a–c)** S_3 mapped using a neighbourhood radius of 3 m; **(d–f)** S_3 mapped using a neighbourhood radius of 5 m. The hollow symbol outlined in blue is from the SE corner of the Rayleigh Peak site, where the rock exposure mapped from the orthophotographs significantly under-predicts the true degree of rock exposure due to a combination vegetation cover and variable insolation conditions.

that although the high-resolution orthophotographs provide the best means of objectively testing our algorithm, the resulting validation data sets are not perfect, and classification errors will result in under-estimation of the success of the roughness metric.

4 Application of the roughness algorithm to transient landscapes – investigating the soil-bedrock transition in Bald Rock Basin, California, and Harrington Creek, Idaho

4.1 Study sites

We investigate the variations in hillslope characteristics exhibited in two landscapes – Bald Rock Basin, in the Californian Sierra Nevada, and the Harrington Creek catchment, a tributary of the Salmon River, Idaho – which both exhibit strongly transient states of landscape evolution, under different climate regimes.

4.1.1 Bald Rock Basin, California

The Bald Rock Basin catchment drains into Middle Fork Feather River, in the north-western Sierra Nevada Mountains, California (Fig. 1c). The regional climate in this locality is strongly seasonal, with maximum (minimum) temperatures range from 30 (12) °C in the summer to 9 (−1) °C in the winter, and mean annual precipitation typically ∼ 1750 mm, a substantial majority of which falls between October and April, whereas the summer months are dry (http://www.prismclimate.org). Geologically, the catchment is underlain by the Bald Rock Pluton, a trondhjemite-tonalite intrusion of mid-late Mesozoic age (Saucedo and Wagner, 1992). The landscape is close to fully vegetated by mixed conifer forest that is typical of the mid-elevation Sierra Nevada (Barbour and Billings, 2000). The notable exception to this is Bald Rock Dome, which rises precipitously from the Feather River Canyon to form a broad, smooth, bare bedrock dome to the north of Bald Rock Basin. Although outside of the study catchment, it hints at the possibility of significant compositional or structural heterogeneity within the pluton that is imposing a localised bottom-up restriction on forest growth in some parts of the landscape (Hahm et al., 2014).

Landscape transience in the Feather River region is driven by a wave of fluvial incision that is presently propagating up the channel network (Hurst et al., 2012). The resultant range of erosion rates spans an order of magnitude, placing fundamental controls on the nature of the hillslopes (Hurst et al., 2012, 2013a), soils (Yoo et al., 2011; Attal et al., 2014; Gabet et al., 2015) and biosphere (Milodowski et al., 2015). Rates of erosion in the inner canyon, driven by fluvial incision along the main-stem Feather River, reach $\sim 250\,\mathrm{mm\,kyr^{-1}}$ (Riebe et al., 2000; Hurst et al., 2012). Bald Rock Basin has not fully adjusted to this elevated rate of fluvial incision, with a prominent topographic knickpoint marking the transition to lower relief topography that is eroding much more slowly at 30–40 $\mathrm{mm\,kyr^{-1}}$ (Riebe et al., 2000; Hurst et al., 2012).

Moving across this gradient in erosion rates, hillslope form changes from being low-gradient and convex to steep and

planar in the rejuvenated parts of the landscape below the knickpoint (Hurst et al., 2012), consistent with the expectations of models of non-linear, diffusion-like sediment transport (Roering et al., 1999). Within Bald Rock Basin itself, Yoo et al. (2011) investigated changes in substrate characteristics between a series of transects across this transition, indicating that the increase in erosion rate drives a reduction in the residence time of material within the weathering zone, highlighted by a decrease in the extent of weathering of both the soil and saprolite. Consistent with these observations, a more detailed inventory of soil grain size distributions from soil pits throughout Bald Rock Basin indicate a marked increase in the coarser grain fraction in more rapidly eroding parts of the basin (Attal et al., 2014). We use the surface roughness algorithm introduced above to expand on this earlier work and further characterise changes in the bedrock exposure across the geomorphic transition.

4.1.2 Harrington Creek, Idaho

The Harrington Creek catchment drains into Main Salmon River, around 40 km SSW of the Bitterroot Mountains, Idaho (Fig. 1d). The regional climate is continental, with maximum (minimum) temperatures ranging from 26.2 (6.2) °C in the summer to 0.0 (−10.8) °C in the winter, whereas precipitation is more evenly distributed throughout the year, with mean annual precipitation typically ∼ 630 mm (http://www.prismclimate.org). Vegetation in the catchment comprises coniferous forest with variable canopy cover (Barbour and Billings, 2000). The catchment is underlain by plutonic rocks related to the Idaho Batholith, with small inclusions of Eocene dykes of rhyolitic-dacitic composition (Lewis and Stanford, 2002). Analysis of fission tracks in apatite and zircon grains from the Idaho Batholith suggest that exhumation rates have varied from 0.03–0.1 mm yr^{-1} between 50–10 Ma to 0.32 ± 0.10 mm yr^{-1} from 10 Ma-present, associated with canyon-forming fluvial incision along the Salmon River (Sweetkind and Blackwell, 1989; Ferrier et al., 2012). Point measurements of regolith production rates, based on cosmogenic ^{10}Be concentrations, suggest erosion rates integrated over 10^3–10^4 years of up to 0.12 mm yr^{-1} (Ferrier et al., 2012). Associated with this fluvial incision are a series of knickpoints that are propagating up the tributaries of the Salmon River, including Harrington Creek, which mark the transition from a slowly eroding, relict landscape to steep, rapidly eroding, rejuvenated topography that is actively adjusting to the elevated incision rates below the fluvial knickpoint (Wood, 2013). The Harrington Creek region has been subject to significantly less research relative to Bald Rock Basin; we use the same methods for this site to investigate changes in the geomorphic characteristics of the hillslopes across this transition.

4.2 Topographic analysis

Changing bedrock exposure across the knickzones was mapped utilising the surface roughness method as described in Sect. 2, using a circular neighbourhood with a radius of 3 m, which was shown to perform well, with limited false positives, in our previous validation (Sect. 3). Topographic gradient was also measured using the slope of the best fitting six term polynomial surface, defined by a least squares regression to a circular neighbourhood with 7 m radius (e.g. Hurst et al., 2012). In order to map changes in hillslope characteristics along the length of the trunk channel, we use longitudinal swath profiles, following a similar approach to the implementation of the generalised swath profile algorithm described by Hergarten et al. (2014), to map each point on the hillslope to the nearest location in the channel network. This method allows frequently used swath profile analysis to be undertaken using curvilinear features, such as river channels, as the baseline rather than requiring linear features. The trunk channels themselves were defined using the DrEICH algorithm (Clubb et al., 2014), which searches for the upstream limit of the topographic signature of fluvial incision to define the fluvial network within the channelised domain. To first order, the longitudinal swath profiles should link hillslopes to the section of channel that sets their lower boundary condition, enabling us to link geomorphic changes in fluvial incision.

4.3 Results

In both Bald Rock Basin (Figs. 9 and 10) and Harrington Creek (Figs. 11 and 12), there are clearly distinct, contrasting topographic domains separated by major knickpoints. Moving across this transition, hillslope morphology changes from low gradient, convex hillslopes (modal gradients above principal knickpoints are ∼ 0.5 and ∼ 0.4 within the headwaters of Bald Rock Basin and Harrington Creek respectively), to steep, planar hillslopes downstream of the knickpoints: respective modal gradients are ∼ 0.9 and ∼ 0.8. However, in addition to the changes in the hillslope profile across this transition there are concomitant textural changes to the hillslopes pertaining to the widespread emergence of bedrock. In both landscapes, the low gradient headwaters are also characterised by smooth topography indicative of a continuous soil mantle: within Bald Rock Basin, 1.5 % of hillslope pixels have $S_3 > 0.010$; < 1 % have $S_3 > 0.015$; within Harrington Creek, 3 % have $S_3 > 0.010$; 1.5 % have $S_3 > 0.015$. In contrast, in the rejuvenated parts of the landscape, the increased dominance of bedrock is indicated by elevated topographic roughness: in the lower reaches of Bald Rock Basin 15 % of hillslope pixels have $S_3 > 0.010$; 7 % have $S_3 > 0.015$, while in the equivalent parts of the Harrington Creek drainage, 29 % have $S_3 > 0.010$; 19 % have $S_3 > 0.015$. Critically, the emergence of bedrock is not uniform across the steeper parts of the landscape. Rather, the steep hillslopes present a rugged patchwork of bedrock outcrops and discontinuous soil cover.

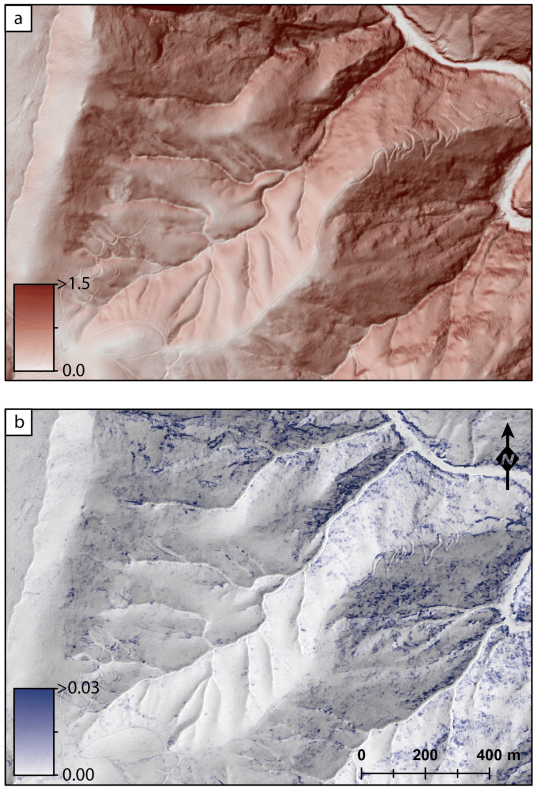

Figure 9. Maps displaying **(a)** topographic slope, and **(b)** S_3 for Bald Rock Basin, Californian Sierra Nevada. The Middle Fork Feather River is located in the NE corner of each map, flowing from NW to SE.

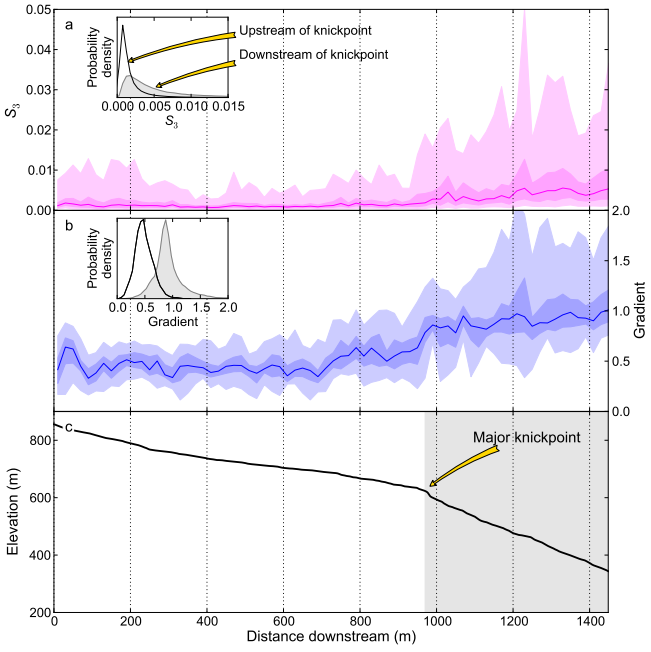

Figure 10. Changes in topographic characteristics along a longitudinal swath centred on the trunk channel draining Bald Rock Basin: **(a)** surface roughness, S_3; **(b)** topographic gradient; **(c)** the longitudinal channel profile. The principal knickpoint has been highlighted, with the inset histograms summarising the distributions of the topographic metrics above and below. Upstream of the major knickpoint, smaller deviations from the typical graded profile indicate a series of smaller knickpoints. The swath has a half width of 250 m, and has been binned into 50 m intervals. In plates **(a)** and **(b)**, the median has been plotted with the shaded intervals bounded by the 25–75th quantiles and 2.5–97.5th quantiles. S_3 was calculated using a 3 m radius neighbourhood window.

Likewise, across the upper part of Bald Rock Basin, there are a number of isolated patches of elevated roughness that can be picked out from the prevailing smooth terrain (Fig. 9). Field Inspection of these selected "rough spots" indicated that they corresponded to isolated rock outcrops, whereas instances of tree throw mounds, which could also generate roughness at short wavelengths, were comparatively rare.

4.4 Discussion

In both Bald Rock Basin and Harrington Creek, topographic knickpoints mark the domain transitions between a slowly eroding "relict" landscape, and rejuvenated topography responding to elevated rates of fluvial incision (Hurst et al., 2012, 2013a; Wood, 2013). Both landscapes exhibit similar hillslope responses to this geomorphic forcing. In this contribution we have deployed our new roughness algorithm to quantify the dynamics of the soil to bedrock transition. Specifically, in both landscapes the transition from soil-mantled to bedrock hillslopes is gradual and patchy. Furthermore, the steep hillslopes do not appear to be completely stripped of soil; the persistence of topographically smooth areas that manage to sustain a forest canopy (Milodowski et al., 2015) indicates that patchy soil cover persists at high erosion rates. In the Feather River Region, aboveground biomass hosted by the hillslopes has been shown to decrease with increasing erosion rates (Milodowski et al., 2015), but biogenic soil production is still able to keep pace with elevated rates of erosion to maintain a partial soil mantle. This is in agreement with observations from soil depth transects within the basin that show little difference in soil depths measured above the knickpoint, ranging from 40–80 cm, to those measured below the knickpoint, which ranged from 30–60 cm (Yoo et al., 2011).

The nature if the soil-bedrock transition observed at these two sites aligns closely with the observations from the San Gabriel Mountains in California (DiBiase et al., 2012). A gradual, patchy transition is significant because it is at odds with the expectations from widely used models of soil production, in which the rate of production decays exponentially with depth from a maximum production rate for a bare bedrock surface (e.g. Heimsath et al., 1997), which in this framework represents a threshold erosion rate defining a sharp transition from soil-mantled to bedrock topog-

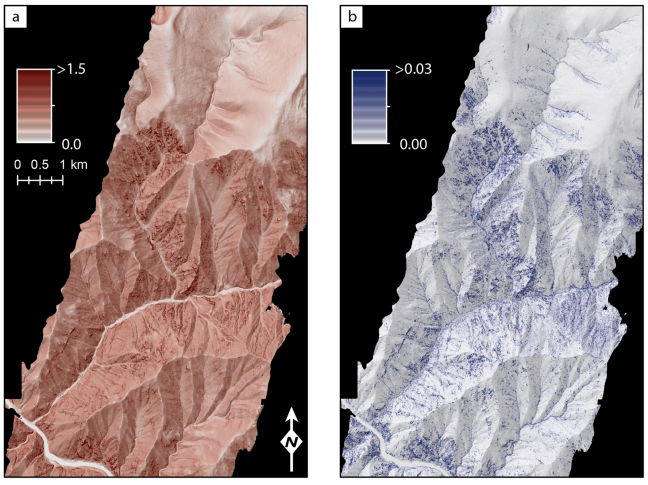

Figure 11. Maps displaying **(a)** topographic slope, and **(b)** S_3, for a sub-catchment of Harrington Creek, Idaho. S_3 was calculated using a 3 m radius neighbourhood window.

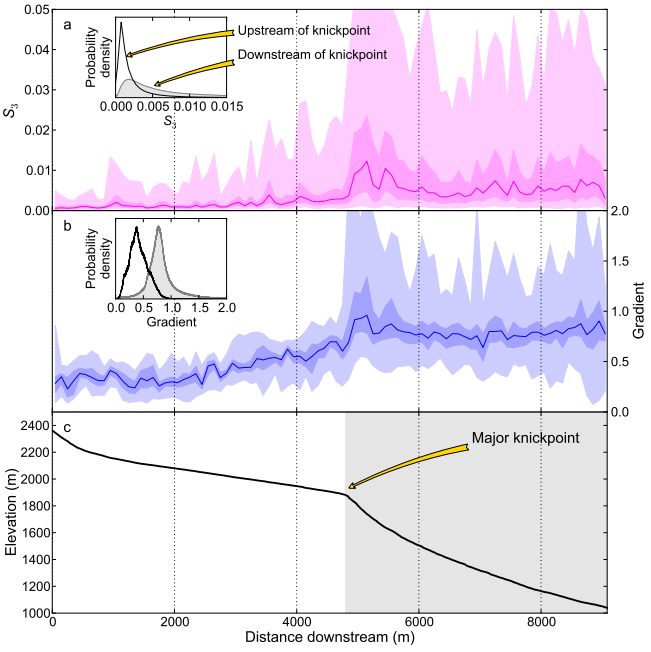

Figure 12. Changes in topographic characteristics along a longitudinal swath centred on the trunk channel draining the principal tributary to Harrington Creek: **(a)** surface roughness, S_3; **(b)** topographic gradient; **(c)** the longitudinal channel profile. The principal knickpoint has been highlighted, with the inset histograms summarising the distributions of the topographic metrics above and below. Upstream of the major knickpoint, smaller deviations from the typical graded profile indicate a series of smaller knickpoints. The swath has a half width of 350 m, and has been binned into 50 m intervals. In plates **(a)** and **(b)**, the median has been plotted along with the shaded intervals bounded by the 25–75th quantiles and 2.5–97.5th quantiles.

raphy. The patchy transition observed may be driven in part by structural or compositional controls on the rate at which bedrock breaks down to form mobile regolith, but can also be rationalised by models of soil production that consider the processes driving soil production and sediment transport as occurring in discrete events (Strudley et al., 2006a, b; Gabet and Mudd, 2010). Understanding whether these patches are stationary in time or dynamic is important in understanding the longer term evolution of steep landscapes and how this evolution is shaped by the coupling of geomorphic and ecological processes. Finally, while clearly important from a hillslope perspective, there are broader implications for landscape evolution: the dynamics of sediment transport in bedrock landscapes are very different to those in soil-mantled landscapes (e.g. Binnie et al., 2007; Dietrich et al., 2003), impacting on the calibre (Attal et al., 2015; Whittaker et al., 2010) and temporal variability (Hovius et al., 2000) of sediment supplied to the channel network; therefore the nature of the soil-bedrock transition impacts on the nature of hillslope-channel coupling, modulating the fluvial response to changes in base level.

5 Overall discussion and conclusions

The structure of topographic relief is controlled by different processes operating at different spatial scales (Perron et al., 2008): at wavelengths greater than ∼ 100 m, topography is dominated by the spacing of ridges and valleys (Perron et al., 2008, 2009); at the sub-hillslope length-scale, other processes generate detectable topographic signatures (e.g. McKean and Roering, 2004; Roering et al., 2010). Booth et al. (2009) exploited spectral analysis to show that areas affected by deep-seated landslides exhibit significantly greater power at intermediate wavelengths (∼ 11–50 m), enabling the objective classification of regions in which deep-seated landslides were prevalent. At shorter length-scales, Roering et al. (2010) suggested that roughness generated at small length-scales (< 7.5 m) in the Oregon Coast Ranges could be attributed to the presence of tree throw mounds; similar analysis of topographic profiles extracted from contrasting catchments in the same setting found a lack of spectral power at these short wavelengths for resistant bedrock hillslopes in comparison to soil-mantled hillslopes, attributed to a diminished biotic contribution to weathering (Marshall and Roering, 2014).

We propose that short wavelength surface roughness, quantified using the same roughness algorithms introduced by McKean and Roering (2004) can be used to make inferences about hillslope characteristics specifically pertaining to the exposure of bedrock. Comparison against rock exposure measured independently and objectively from high-resolution orthophotographs from multiple landscapes suggests that the emergence of bedrock in hillslopes produces a detectable topographic signature that distinguishes it from

hillslopes that have a continuous soil mantle. We applied this technique to forested landscapes in California and Idaho, highlighting the ability of LiDAR surveys to resolve high-resolution features of the topography through canopy. For obvious reasons validation is simpler in un-vegetated terrain but prior to the introduction of below-canopy UAVs for data collection, we suggest our method is adequate for use in vegetated terrain. Users should validate using field observations to avoid false positives from, for example, tree throw mounds. Thus we propose surface roughness as a new method for mapping rock exposure from LiDAR data that complements previously published metrics (DiBiase et al., 2012), and is likely to be of particular benefit in landscapes in which rock outcrops are present at topographic gradients lower than the angle of repose.

We caveat this finding with the statement that rock exposure is not the only mechanism of generating topographic roughness at short length-scales; for example, gullying and slumping provide two mechanisms by which the smooth parabolic morphology associated with ideal, diffusive soil-mantled hillslopes may be modified (Tarolli and Dalla Fontana, 2009); likewise small-scale features associated with deep-seated landslides, such as folds and scarps, generate a roughness signal at similar length-scales to rock outcrop (McKean and Roering, 2004; Tarolli et al., 2010). In addition, while many soil-mantled sediment transport processes act to diffuse topography, they typically do so through discrete events (e.g. tree throw) (Furbish et al., 2009; Gabet and Mudd, 2010), and while the fingerprint that these individual events leave on the landscape is transient, they provide a potentially important roughness signature at the relevant length-scale for that mode of disturbance (Roering et al., 2010). An additional factor to consider is that bedrock morphology is itself variable, and therefore certain mechanisms of generating rock exposure may not generate significant roughness; this would be exemplified by, for example, low gradient, glacially polished surfaces, or by massive granitoid bedrock with very low fracture density in which jointing is restricted to approximately surface parallel exfoliation planes. Consequently, interpretation of surface roughness metrics should critically take into account the presence of other geomorphic processes that are potentially operating within the landscape and the characteristics of the bedrock itself. Indeed, this principal applies to the interpretation of any topographic metric obtained from remotely sensed data; in complex geomorphic settings, isolation of specific hillslope characteristics from a single textural attributes may be impossible at the data resolution presently available from airborne surveys; ultimately a combination of metrics, covering a broader range of morphological characteristics may well be necessary.

The characterisation of hillslopes is of importance across a diverse range of surface processes research, providing a better understanding of controls on hydrological flow routing, sediment production and transport processes and ecosystem development. The utility of topographic data to aid this endeavour is strongly dependent on the resolution of these data sets. In the case of hillslope characteristics, such as rock exposure, roughness is expressed at the metre scale; using 1 m resolution digital elevation models, it is possible to examine variations in hillslope form at sufficient levels of detail that it is possible to distinguish between soil and bedrock hillslopes; this information is rapidly lost as the data resolution is coarsened (DiBiase et al., 2012). However these shorter length scales are particularly susceptible to noise in the data set (Albani et al., 2004; Sofia et al., 2013). This highlights the requirement for high quality, high resolution, which permit accurate classification of vegetation and ground returns prior to surface creation. LiDAR surveys with higher shot spacing are therefore likely to provide a disproportionately greater level of detail on hillslope characteristics (Brodu and Lague, 2012), and this should be taken into account when planning airborne surveys. In particular, the continued development of unmanned aerial vehicles (UAVs) as a platform for airborne LiDAR collection will increasingly make higher resolution surveys accessible to the research community (e.g. Lin et al., 2011).

Finally, from our analysis of the geomorphic changes associated with changing rates of erosion in two different landscapes reveals a number of significant conclusions regarding the nature of the soil-bedrock transition. In both cases, the transition from soil-mantled hillslopes to bedrock dominated hillslopes is clearly gradual, with areas of patchy soil coverage persistent on steep, rapidly eroding hillslopes. A "patchy" transition from soil-mantled to bedrock hillslopes challenges prevailing modelling approaches towards soil production, but is in agreement with conclusions from previous studies of soil production in rapidly eroding landscapes – the European Alps (Norton et al., 2008), San Gabriel Mountains, California (Heimsath et al., 2012) and Southern Alps, New Zealand (Larsen et al., 2014) – each of which observe the coexistence of soil and bedrock on rapidly eroding hillslopes. This has been attributed in part to efficient biogenic soil production (Larsen et al., 2014), which facilitates the rapid generation and stabilisation of soil between landslide events, and lithological susceptibility to weathering processes (Norton et al., 2008). The hypothesis of a biogenically mediated soil-bedrock transition is supported by the observation in these landscapes that patchy vegetation cover persists on the steeper hillslopes where trees have maintained a foothold, and is in agreement with expectations from numerical modelling of soil production by discrete events (Gabet and Mudd, 2010). Capturing the salient aspects of these models within larger-scale landscape evolution models represents a key challenge in simulating the evolution of mixed-bedrock landscapes that are typical of many upland settings.

Software availability

We have made our bedrock detection software available through the community sediment dynamics modelling system (CSDMS) website; source code may be downloaded at http://csdms.colorado.edu/wiki/Model:SurfaceRoughness.

The Supplement related to this article is available online at doi:10.5194/esurf-3-483-2015-supplement.

Author contributions. D. T. Milodowski and S. M. Mudd the algorithms and wrote the code. D. T. Milodowski, S. M. Mudd and E. T. A. Mitchard performed the analysis and wrote the paper.

Acknowledgements. This research was funded by a NERC studentship (NERC DTG NE/152830X/1 and NE/J500021/1; DTM), in addition to the Harkness Award from the University of Cambridge (DTM). ETAM is funded by a NERC Fellowship (NE/I021217/1). SMM is supported by U.S. Army Research Office contract number W911NF-13-1-0478. The authors would like to thank Emmanuel Gabet, Dimitri Lague, Stuart Grieve, and Fiona Clubb for valuable discussions that facilitated the development of this research.

Edited by: J. Willenbring

References

Albani, M., Klinkenberg, B., Andison, D. W., and Kimmins, J. P.: The choice of window size in approximating topographic surfaces from Digital Elevation Models, Int. J. Geogr. Inf. Sci., 18, 577–593, doi:10.1080/13658810410001701987, 2004.

Anderson, R. S.: Modeling the tor-dotted crests, bedrock edges, and parabolic profiles of high alpine surfaces of the Wind River Range, Wyoming, Geomorphology, 46, 35–58, doi:10.1016/S0169-555X(02)00053-3, 2002.

Attal, M., Mudd, S. M., Hurst, M. D., Weinman, B., Yoo, K., and Naylor, M.: Impact of change in erosion rate and landscape steepness on hillslope and fluvial sediments grain size in the Feather River basin (Sierra Nevada, California), Earth Surf. Dynam., 3, 201–222, doi:10.5194/esurf-3-201-2015, 2015.

Barbour, M. G. and Billings, W. D.: North American Terrestrial Vegetation, edited by: Barbour, M. G. and Billings, W. D., Cambridge University Press, Cambridge, UK, New York, NY, USA, 2000.

Binnie, S. A., Phillips, W. M., Summerfield, M. A., and Fifield, L. K.: Tectonic uplift, threshold hillslopes, and denudation rates in a developing mountain range, Geology, 35, 743–746, doi:10.1130/G23641A.1, 2007.

Booth, A. M., Roering, J. J., and Perron, J. T.: Automated landslide mapping using spectral analysis and high-resolution topographic data: Puget Sound lowlands, Washington, and Portland Hills, Oregon, Geomorphology, 109, 132–147, doi:10.1016/j.geomorph.2009.02.027, 2009.

Brodu, N. and Lague, D.: 3D terrestrial lidar data classification of complex natural scenes using a multi-scale dimensionality criterion: Applications in geomorphology, ISPRS J. Photogramm., 68, 121–134, doi:10.1016/j.isprsjprs.2012.01.006, 2012.

Carson, M. A. and Kirkby, M. J.: Hillslope form and process, Cambridge University Press, Cambridge, UK, 1972.

Cavalli, M., Tarolli, P., Marchi, L., and Dalla Fontana, G.: The effectiveness of airborne LiDAR data in the recognition of channel-bed morphology, CATENA, 73, 249–260, doi:10.1016/j.catena.2007.11.001, 2008.

Chorover, J., Troch, P. A., Rasmussen, C., Brooks, P. D., Pelletier, J. D., Breshars, D. D., Huxman, T. E., Kurc, S. A., Lohse, K. A., McIntosh, J. C., Meixner, T., Schaap, M. G., Litvak, M. E., Perdrial, J., Harpold, A., and Durcik, M.: How Water, Carbon, and Energy Drive Critical Zone Evolution: The Jemez–Santa Catalina Critical Zone Observatory, Vadose Zone J., 10, 884–899, doi:10.2136/vzj2010.0132, 2011.

Clubb, F. J., Mudd, S. M., Milodowski, D. T., Hurst, M. D., and Slater, L. J.: Objective extraction of channel heads from high-resolution topographic data, Water Resour. Res., 50, 4283–4304, doi:10.1002/2013WR015167, 2014.

Colby, J.: Topographic Normalization in Rugged Terrain, Photogramm. Eng. Rem., 57, 531–537, 1991.

Culling, W.: Soil Creep and the Development of Hillside Slopes, J. Geol., 71, 127–161, 1963.

Culling, W. E. H.: Theory of Erosion on Soil-Covered Slopes, J. Geol., 73, 230–254, 1965.

DiBiase, R. A., Heimsath, A. M., and Whipple, K. X.: Hillslope response to tectonic forcing in threshold landscapes, Earth Surf. Proc. Land., 37, 855–865, doi:10.1002/esp.3205, 2012.

DiBiase, R. A. and Lamb, M. P.: Vegetation and wildfire controls on sediment yield in bedrock landscapes, Geophys. Res. Lett., 40, 1093–1097, doi:10.1002/grl.50277, 2013.

Dietrich, W. E., Bellugi, D. G., Sklar, L. S., Stock, J. D., Heimsath, A. M., and Roering, J. J.: Geomorphic transport laws for predicting landscape form and dynamics, Geophys. Monogr.-Am. Geophys. UNION, 135, 103–132, 2003.

Evans, I. S.: An integrated system of terrain analysis and slope mapping, Z. Geomorphol, 36, 274–295, 1980.

Evans, J. S. and Hudak, A. T.: A Multiscale Curvature Algorithm for Classifying Discrete Return LiDAR in Forested Environments, IEEE T. Geosci. Remote, 45, 1029–1038, doi:10.1109/TGRS.2006.890412, 2007.

Fara, H. D. and Scheidegger, A. E.: An eigenvalue method for the statistical evaluation of fault plane solutions of earthquakes, B. Seismol. Soc. Am., 53, 811–816, 1963.

Ferrier, K. L., Kirchner, J. W., and Finkel, R. C.: Weak influences of climate and mineral supply rates on chemical erosion rates: measurements along two altitudinal transects in the Idaho Batholith, J. Geophys. Res.-Earth, 117, F02026, doi:10.1029/2011JF002231, 2012.

Furbish, D. J., Hamner, K. K., Schmeeckle, M., Borosund, M. N., and Mudd, S. M.: Rain splash of dry sand revealed by high-speed imaging and sticky paper splash targets, J. Geophys. Res.-Earth, 112, F01001, doi:10.1029/2006JF000498, 2007.

Furbish, D. J., Haff, P. K., Dietrich, W. E., and Heimsath, A. M.: Statistical description of slope-dependent soil transport and the diffusion-like coefficient, J. Geophys. Res., 114, F00A05, doi:10.1029/2009JF001267, 2009.

Furbish, D. J. and Roering, J. J.: Sediment disentrainment and the concept of local vs. nonlocal transport on hillslopes, J. Geophys. Res.-Earth, 118, 937–952, doi:10.1002/jgrf.20071, 2013.

Gabet, E. J.: Sediment transport by dry ravel, J. Geophys. Res.-Sol. Ea., 108, 2049, doi:10.1029/2001JB001686, 2003.

Gabet, E. J., Reichman, O. J., and Seabloom, E. W.: The effects of bioturbation on soil processes and sediment transport, Annu. Rev. Earth Pl. Sc., 31, 249–273, 2003.

Gabet, E. J. and Mudd, S. M.: Bedrock erosion by root fracture and tree throw: A coupled biogeomorphic model to explore the humped soil production function and the persistence of hillslope soils, J. Geophys. Res., 115, F04005, doi:10.1029/2009JF001526, 2010.

Gabet, E. J., Mudd, S. M., Milodowski, D. T., Yoo, K., Hurst, M. D., and Dosseto, A.: Local topography and erosion rate control regolith thickness along a ridgeline in the Sierra Nevada, California, Earth Surf. Proc. Land., 40, 1779–1790, doi:10.1002/esp.3754, 2015.

Gilbert, G.: The convexity of hilltops, J. Geol., 17, 344–350, 1909.

Goodfellow, B. W., Chadwick, O. A., and Hilley, G. E.: Depth and character of rock weathering across a basaltic-hosted climosequence on Hawai'i, Earth Surf. Proc. Land., 39, 381–398, doi:10.1002/esp.3505, 2014a.

Goodfellow, B. W., Skelton, A., Martel, S. J., Stroeven, A. P., Jansson, K. N., and Hättestrand, C.: Controls of tor formation, Cairngorm Mountains, Scotland, J. Geophys. Res.-Earth., 119, 2013JF002862, doi:10.1002/2013JF002862, 2014b.

Graham, R., Rossi, A., and Hubbert, R.: Rock to regolith conversion: producing hospitable substrates for terrestrial ecosystems, GSA Today, 20, 4–9, doi:10.1130/GSAT57A.1, 2010.

Hahm, W. J., Riebe, C. S., Lukens, C. E. and Araki, S.: Bedrock composition regulates mountain ecosystems and landscape evolution, P. Natl. Acad. Sci. USA, 111, 3338–3343, doi:10.1073/pnas.1315667111, 2014.

Hale, S. R. and Rock, B. N.: Impact of topographic normalization on land-cover classification accuracy, Photogramm. Eng. Rem. S., 69, 785–791, doi:10.14358/PERS.69.7.785, 2003.

Heimsath, A., Dietrich, W., Nishiizumi, K., and Finkel, R.: The soil production function and landscape equilibrium, Nature, 388, 358–361, doi:10.1038/41056, 1997.

Heimsath, A. M., DiBiase, R. A., and Whipple, K. X.: Soil production limits and the transition to bedrock-dominated landscapes, Nat. Geosci., 5, 210–214, doi:10.1038/ngeo1380, 2012.

Hergarten, S., Robl, J., and Stüwe, K.: Extracting topographic swath profiles across curved geomorphic features, Earth Surf. Dynam., 2, 97–104, doi:10.5194/esurf-2-97-2014, 2014.

Hovius, N., Stark, C. P., Hao-Tsu, C., and Jiun-Chuan, L.: Supply and removal of sediment in a landslide-dominated mountain belt: Central Range, Taiwan, J. Geol., 108, 73–89, 2000.

Hurst, M. D., Mudd, S. M., Walcott, R., Attal, M., and Yoo, K.: Using hilltop curvature to derive the spatial distribution of erosion rates, J. Geophys. Res.-Earth, 117, F02017, doi:10.1029/2011JF002057, 2012.

Hurst, M. D., Mudd, S. M., Yoo, K., Attal, M., and Walcott, R.: Influence of lithology on hillslope morphology and response to tectonic forcing in the northern Sierra Nevada of California, J. Geophys. Res.-Earth, 118, 832–851, doi:10.1002/jgrf.20049, 2013a.

Hurst, M. D., Mudd, S. M., Attal, M., and Hilley, G.: Hillslopes Record the Growth and Decay of Landscapes, Science, 341, 868–871, doi:10.1126/science.1241791, 2013b.

Lague, D., Brodu, N., and Leroux, J.: Accurate 3D comparison of complex topography with terrestrial laser scanner: Application to the Rangitikei canyon (N-Z), ISPRS J. Photogramm., 82, 10–26, doi:10.1016/j.isprsjprs.2013.04.009, 2013.

Larsen, I. J., Almond, P. C., Eger, A., Stone, J. O., Montgomery, D. R., and Malcolm, B.: Rapid Soil Production and Weathering in the Western Alps, New Zealand, Science, 343, 637–640, doi:10.1126/science.1244908, 2014.

Lashermes, B., Foufoula-Georgiou, E., and Dietrich, W. E.: Channel network extraction from high resolution topography using wavelets, Geophys. Res. Lett., 34, L23S04, doi:10.1029/2007GL031140, 2007.

Lewis, R. S. and Stanford, L. R.: Geologic map compilation of the western half of the Nez Perce Pass 30×60 min quadrangle, Idaho Geological Survey, Idaho, USA, 2002.

Lin, Y., Hyyppa, J., and Jaakkola, A.: Mini-UAV-Borne LIDAR for Fine-Scale Mapping, IEEE Geosci. Remote S., 8, 426–430, doi:10.1109/LGRS.2010.2079913, 2011.

Lin, C.-W., Tseng, C.-M., Tseng, Y.-H., Fei, L.-Y., Hsieh, Y.-C., and Tarolli, P.: Recognition of large scale deep-seated landslides in forest areas of Taiwan using high resolution topography, J. Asian Earth Sci., 62, 389–400, doi:10.1016/j.jseaes.2012.10.022, 2013.

Marshall, J. A. and Roering, J. J.: Diagenetic variation in the Oregon Coast Range: Implications for rock strength, soil production, hillslope form, and landscape evolution, J. Geophys. Res.-Earth, 119, 1395–1417, doi:10.1002/2013JF003004, 2014.

McKean, J. A., Dietrich, W. E., Finkel, R. C., Southon, J. R., and Caffee, M. W.: Quantification of soil production and downslope creep rates from cosmogenic 10Be accumulations on a hillslope profile, Geology, 21, 343–346, doi:10.1130/0091-7613(1993)021<0343:QOSPAD>2.3.CO;2, 1993.

McKean, J. and Roering, J.: Objective landslide detection and surface morphology mapping using high-resolution airborne laser altimetry, Geomorphology, 57, 331–351, doi:10.1016/S0169-555X(03)00164-8, 2004.

Migon, P.: Granite Landscapes of the World, Oxford University Press, Oxford, UK, 2006.

Milodowski, D. T., Mudd, S. M., and Mitchard, E. T. A.: Erosion rates as a potential bottom-up control of forest structural characteristics in the Sierra Nevada Mountains, Ecology, 96, 31–38, doi:10.1890/14-0649.1, 2015.

Moody, J. A. and Martin, D. A.: Initial hydrologic and geomorphic response following a wildfire in the Colorado Front Range, Earth Surf. Proc. Land., 26, 1049–1070, doi:10.1002/esp.253, 2001.

Norton, K. P., von Blanckenburg, F., Schlunegger, F., Schwab, M., and Kubik, P. W.: Cosmogenic nuclide-based investigation of spatial erosion and hillslope channel coupling in the transient foreland of the Swiss Alps, Geomorphology, 95, 474–486, doi:10.1016/j.geomorph.2007.07.013, 2008.

Passalacqua, P., Trung, T. D., Foufoula-Georgiou, E., Sapiro, G., and Dietrich, W. E.: A geometric framework for channel network extraction from lidar: Nonlinear diffusion and geodesic paths, J. Geophys. Res., 115, F01002, doi:201010.1029/2009JF001254, 2010.

Pelletier, J. D.: A robust, two-parameter method for the extraction of drainage networks from high-resolution digital elevation models

(DEMs): Evaluation using synthetic and real-world DEMs, Water Resour. Res., 49, 75–89, doi:10.1029/2012WR012452, 2013.

Pelletier, J. D. and Rasmussen, C.: Quantifying the climatic and tectonic controls on hillslope steepness and erosion rate, Lithosphere, 1, 73–80, doi:10.1130/L3.1, 2009.

Perron, J. T., Kirchner, J. W., and Dietrich, W. E.: Spectral signatures of characteristic spatial scales and nonfractal structure in landscapes, J. Geophys. Res.-Earth, 113, F04003, doi:10.1029/2007JF000866, 2008.

Perron, J. T., Kirchner, J. W., and Dietrich, W. E.: Formation of evenly spaced ridges and valleys, Nature, 460, 502–505, doi:10.1038/nature08174, 2009.

Phillips, J. D. and Marion, D. A.: Pedological memory in forest soil development, Forest Ecol. Manag., 188, 363–380, doi:10.1016/j.foreco.2003.08.007, 2004.

Pirotti, F. and Tarolli, P.: Suitability of LiDAR point density and derived landform curvature maps for channel network extraction, Hydrol. Process., 24, 1187–1197, doi:10.1002/hyp.7582, 2010.

Riebe, C. S., Kirchner, J. W., Granger, D. E., and Finkel, R. C.: Erosional equilibrium and disequilibrium in the Sierra Nevada, inferred from cosmogenic 26Al and 10Be in alluvial sediment, Geology, 28, 803–806, 2000.

Roering, J. J., Kirchner, J. W., and Dietrich, W. E.: Evidence for nonlinear, diffusive sediment transport on hillslopes and implications for landscape morphology, Water Resour. Res., 35, 853–870, doi:10.1029/1998WR900090, 1999.

Roering, J. J., Marshall, J., Booth, A. M., Mort, M., and Jin, Q.: Evidence for biotic controls on topography and soil production, Earth Planet. Sc. Lett., 298, 183–190, doi:10.1016/j.epsl.2010.07.040, 2010.

Ruleman, C. A., Bohannon, R. G., Bryant, B., Shroba, R. R., and Premo, W. R.: Geologic Map of the Bailey $30' \times 60'$ Quadrangle, North-Central Colorado, US Geological Survey, Denver, Colorado, USA, 2011.

Saucedo, G. J. and Wagner, D. L.: Geologic Map of the Chico Quadrangle, California Department of Conservation, Division of Mines and Geology, Sacramento, California, USA, 1992.

Sheffer, E., von Hardenberg, J., Yizhaq, H., Shachak, M., and Meron, E.: Emerged or imposed: a theory on the role of physical templates and self-organisation for vegetation patchiness, Ecol. Lett., 16, 127–139, doi:10.1111/ele.12027, 2013.

Smith, T. B., Wayne, R. K., Girman, D. J., and Bruford, M. W.: A Role for Ecotones in Generating Rainforest Biodiversity, Science, 276, 1855–1857, doi:10.1126/science.276.5320.1855, 1997.

Sofia, G., Tarolli, P., Cazorzi, F., and Dalla Fontana, G.: An objective approach for feature extraction: distribution analysis and statistical descriptors for scale choice and channel network identification, Hydrol. Earth Syst. Sci., 15, 1387–1402, doi:10.5194/hess-15-1387-2011, 2011.

Sofia, G., Pirotti, F., and Tarolli, P.: Variations in multiscale curvature distribution and signatures of LiDAR DTM errors, Earth Surf. Proc. Land., 38, 1116–1134, doi:10.1002/esp.3363, 2013.

Sofia, G., Fontana, G. D., and Tarolli, P.: High-resolution topography and anthropogenic feature extraction: testing geomorphometric parameters in floodplains, Hydrol. Process., 28, 2046–2061, doi:10.1002/hyp.9727, 2014.

Strudley, M. W., Murray, A. B., and Haff, P. K.: Emergence of pediments, tors, and piedmont junctions from a bedrock weathering–regolith thickness feedback, Geology, 34, 805–808, doi:10.1130/G22482.1, 2006a.

Strudley, M. W., Murray, A. B., and Haff, P. K.: Regolith thickness instability and the formation of tors in arid environments, J. Geophys. Res.-Earth, 111, F03010, doi:10.1029/2005JF000405, 2006b.

Sweetkind, D. S. and Blackwell, D. D.: Fission-track evidence of the Cenozoic thermal history of the Idaho batholith, Tectonophysics, 157, 241–250, doi:10.1016/0040-1951(89)90142-X, 1989.

Tarolli, P. and Dalla Fontana, G.: Hillslope-to-valley transition morphology: New opportunities from high resolution DTMs, Geomorphology, 113, 47–56, doi:10.1016/j.geomorph.2009.02.006, 2009.

Tarolli, P., Sofia, G., and Fontana, G. D.: Geomorphic features extraction from high-resolution topography: landslide crowns and bank erosion, Nat. Hazards, 61, 65–83, doi:10.1007/s11069-010-9695-2, 2010.

Teillet, P. M., Guindon, B., and Goodenough, D. G.: On the slope-aspect correction of multispectral scanner data, Can. J. Remote Sens., 8, 84–106, 1982.

Todd, V. R., Alvarez, R. M., and Techni Graphic Systems, Inc.: Preliminary geologic map of the El Cajon $30' \times 60'$ quadrangle, southern California, US Geological Survey, Menlo Park, California, USA, 2004.

Watson, G. S.: Statistics of orientation data, J. Geol., 74, 786–797, 1966.

Whelley, P. L., Glaze, L. S., Calder, E. S., and Harding, D. J.: LiDAR-Derived Surface Roughness Texture Mapping: Application to Mount St. Helens Pumice Plain Deposit Analysis, IEEE T. Geosci. Remote, 52, 426–438, doi:10.1109/TGRS.2013.2241443, 2014.

Whittaker, A. C., Attal, M., and Allenn, P. A.: Characterising the origin, nature and fate of sediment exported from catchments perturbed by active tectonics, Basin Res., 22, 809–828, doi:10.1111/j.1365-2117.2009.00447.x, 2010.

Wilkinson, M. T., Chappell, J., Humphreys, G. S., Fifield, K., Smith, B., and Hesse, P.: Soil production in heath and forest, Blue Mountains, Australia: influence of lithology and palaeoclimate, Earth Surf. Proc. Land., 30, 923–934, doi:10.1002/esp.1254, 2005.

Woodcock, N. H.: Specification of Fabric Shapes Using an Eigenvalue Method, Geol. Soc. Am. Bull., 88, 1231–1236, doi:10.1130/0016-7606(1977)88<1231:SOFSUA>2.0.CO;2, 1977.

Wood, R.: Transient hillslope response to an incision wave sweeping up a watershed: a case study from the Salmon River, Masters Theses, available at: http://scholarworks.sjsu.edu/etd_theses/4322 (last access: 14 October 2015), 2013.

Wu, T. F., Lin, C. J., and Weng, R. C.: Probability estimates for multi-class classification by pairwise coupling, J. Mach. Learn. Res., 5, 975–1005, 2004.

Yoo, K., Amundson, R., Heimsath, A. M., and Dietrich, W. E.: Process-based model linking pocket gopher (Thomomys bottae) activity to sediment transport and soil thickness, Geology, 33, 917–920, doi:10.1130/G21831.1, 2005.

Yoo, K., Weinman, B., Mudd, S. M., Hurst, M., Attal, M., and Maher, K.: Evolution of hillslope soils: The geomorphic theater and the geochemical play, Appl. Geochem., 26, S149–S153, 2011.